Journal of Glaciology

Article

Cite this article: Cao P, Chen Z, Cao H, Chen B, Zheng Z (2020). Anti-icing performance of hydrophobic material used for electromechanical drill applied in ice core drilling. *Journal of Glaciology* **66**(258), 618–626. https://doi.org/10.1017/jog.2020.33

Received: 30 November 2019
Revised: 10 April 2020
Accepted: 14 April 2020
First published online: 10 June 2020

Key words:
Anti-icing; hydrophobic coating; ice adhesion strength; ice core drilling; warm ice

Author for correspondence:
Zhichuan Zheng,
E-mail: zhengzc@jlu.edu.cn

cambridge.org/jog

Anti-icing performance of hydrophobic material used for electromechanical drill applied in ice core drilling

Pinlu Cao, Zhuo Chen, Hongyu Cao, Baoyi Chen and Zhichuan Zheng

Polar Research Center, Jilin University, No. 938 Ximinzhu Str., Changchun City 130061, China

Abstract

Using an anti-icing coating to prevent ice accretion on the drill surface is a feasible solution to address the drilling difficulties in warm ice. In this study, four types of commercially available hydrophobic coating materials were tested to evaluate their water repellency and anti-icing properties, namely, a mixture of silica and fluorocarbon resin with polytrifluoroethylene, modified Teflon, silica-based emulsion and an acrylic-based copolymer. Their water contact angles are ~107°, 101°, 114° and 95°, respectively. All these hydrophobic coatings can significantly reduce the strength of the ice adhesion within a temperature range of −10 to −30°C on a planar or curved surface. The coating of an acrylic-based copolymer, in particular, can reduce the average tensile strength and the shear strength of the ice adhesion by 87.08 and 97.11% on planar surfaces at −30°C, and by 98.06 and 96.15% on a curved surface, respectively. The main challenge in the practical application of these coatings is their durability. An acrylic-based copolymer coating will lose its water repellency performance after 140 cycles of abrasion. The shear strength of ice adhered on curved surfaces coated with this material will approach that achieved on uncoated surfaces after 11 cycles of icing and de-icing tests.

1. Introduction

Drilling into the basal ice and subglacial environment of large ice sheets for sample recovery is of great scientific interest. It can provide a rich paleo-environmental archive for numerous types of studies including understanding the mechanism of global climate change, learning about the evolution of the earth's glaciology and determining the resilience of life forms exposed to extreme conditions. Sampling from these zones is also important to provide scientists with information regarding the ice-sheet/bedrock interaction and how this zone influences the overlying ice-sheet dynamics (Popp and others, 2014a; Cao and others, 2018). However, the ice located in this zone is extremely difficult to drill with electromechanical drills because the in situ temperature of the ice is close to or at its pressure melting point, which is a so-called warm ice problem. During the process of ice cutting, ice chips that partially melted owing to the cutting heat refreeze, blocking the pathway of chips into the chip chamber. In addition, refrozen ice builds up on the cutters and shoes of the drill bit. The performance of the drill rapidly deteriorates, which not only lowers the penetration rate, but also leads to a poor core recovery and frequent drill sticking (Augustin and others, 2007; Cao and others, 2015).

There have been numerous attempts to solve this icing problem in warm ice drilling. For example, an ethanol–water solution has been successfully used to dissolve refrozen ice at several deep drilling sites, such as NorthGRIP, Greenland, EPICA Dome C and EPICA Droning Maud Land in Antarctica (Johnsen and others, 2007). However, the use of an ethanol–water solution generates its own set of problems such as a partial dissolution of the ice core, sticking of the core in the core barrel and the formation of clathrate hydrate when HCFC 141b is used as a densifier in the drilling fluid (Johnsen and others, 2007; Murshed and others, 2007). A new geometry of cutters was used in hole No. 5 in Vostok station to overcome drilling difficulties in warm ice. The bottom of the cutter was designed to have a dihedral shape to increase the clearance angle, and several slots were also designed to allow the ice chips to be more easily conducted off the borehole bottom. It seems that the drilling problem was solved because the run length increased in spite of a poor penetration rate (Vasiliev and others, 2007). However, this was unable to improve the drill performance during later testing in the EPICA Dome C-2 borehole. To reduce the sticking of ice chips and prevent adherence to the surface of the cutters, Zagorodnov and others (2005) suggested the use of staggered cutters to drill into warm ice. This was then tested at Vostok station and later at the NEEM borehole. The results indicated that these staggered cutters can produce coarser chips that are less sticky and easier to transport from the borehole bottom and clean from the drill at the surface (Popp and others, 2014b; Talalay and others, 2015). A special short Teflon-coated drill was used in Dome Fuji to make the drill more effective in warm ice environments by avoiding ice adhesion; it achieved good results, although the duration of the drilling was not long (Motoyama, 2007). Similarly, a dolphin mount coated with Teflon was successfully used in warm ice in Aurora Peak, central Alaska (Matoba and others, 2014). It not only reduced the friction between the ice and cutters, but also effectively protected the drill from ice accretion on its surface. Therefore, using an

anti-icing coating to prevent ice accretion may be one feasible solution to reduce the drilling problems in warm ice. Even if it cannot be applied as a standalone solution to the icing problem, the integration of suitable coatings on the drill surface can enhance the effectiveness of other anti-icing measures.

In fact, icing is a common problem in many different areas such as aeronautics, electric power transmission lines, wind turbines, marine vessels, buildings and oil platforms. The formation of ice on these surfaces can cause system malfunctions, which results in large economic losses, or even severe accidents. One particularly attractive technique to address this problem is anti-icing coatings that modify the surface topography and inhibit the formation and accumulation of ice (Jung and others, 2015). Owing to their convenience and simplicity, the use of hydrophobic surfaces, which originate from natural microstructures such as the surfaces of lotus leaves and rose petals, is regarded as one of the most promising approaches to achieving an anti-icing coating and have frequently been applied in the above fields (Barthlott and Neinhuis, 1997; He and others, 2015). Compared with a normal hydrophilic surface, a hydrophobic surface has a high water contact angle and a low roll angle owing to its high water repellency property. A water droplet on a hydrophobic surface does not touch a large area of the surface like that on a hydrophilic surface and adopts a spherical shape, thus making the water contact angle extremely large, allowing it to easily drop off the surface (Fillion and others, 2014). In addition to extraordinary water repellency, a hydrophobic surface can reduce the accumulation of ice and even completely prevent its formation. For example, Cao and others (2009) reported low ice accumulation on hydrophobic nanoparticle–polymer composite surfaces exposed to freezing rain conditions. In a study by Liu and others (2008), a superhydrophobic surface has a strong ability to restrain frost growth and can retard frost formation to a certain extent, allowing the frost layer to be easily removed. Beyond these performance advantages, a hydrophobic surface can also significantly reduce the strength of the ice adhesion. Farhadi and others (2011) investigated the anti-icing performance of several micro/nano-rough hydrophobic coatings with a different surface chemistry and topography and found that superhydrophobic surfaces exhibit a significantly lower ice adhesion strength than that on polished aluminum. In a study by Bharathidasan and others (2014), the ice-adhesion strength on silicon-based hydrophobic surfaces was ~43 times lower than that on normal hydrophilic surfaces such as polymethylmethacrylate and polyurethane coatings. In fact, ice adhesion strength can be affected by numerous factors including environmental parameters (such as temperature and atmospheric conditions), substrate characteristics and properties (such as roughness, geometry, stiffness, water contact angle and thermal expansion coefficient), ice properties (such as ice strength and liquid water content) and the measurement method (Guerin and others, 2016). Owing to the complexity of ice adhesion, numerous related phenomena remain unexplained. In particular, the reasons why hydrophobic coatings can prevent ice accumulation and reduce ice adhesion strength are poorly understood. Despite this, the use of a low-adhesion coating remains a better choice as it is an extremely effective method to solve the ice problem in numerous cases.

The excellent water repellency and anti-icing properties of hydrophobic surfaces are perfect for warm ice drilling. If the down-hole equipment of an electromechanical drill is coated with a hydrophobic or superhydrophobic material, it will not allow the meltwater or partially melted ice chips to remain on its surface. Thus, the drill can maintain a good performance in a warm ice environment. Even if the meltwater or ice chips refreeze on the surface of the drill, they can be easily sheared off the surface owing to the lower ice adhesion force, which can reduce or eliminate the accumulation of ice. Accordingly, the risk of a stuck drill can be significantly reduced or completely avoided. Therefore, choosing a suitable hydrophobic material to coat the surface of the drill is a promising method to solve the drilling difficulties that occur in warm ice.

Numerous chemical modification materials such as fluoroalkyl silane, Teflon and fatty acids have been used to fabricate a hydrophobic coating (Hu and others, 2010; Bernagozzi and others, 2014; Park and others, 2019). Such coatings can be applied to a variety of engineering materials including alloys, wood, plastics, glass and metals used as substrates (Chen and others, 2018; Hasegawa and others, 2018; Kim and others, 2019). Despite the availability of several types of commercial hydrophobic coating materials in China, most cannot be used on a steel material surface. In this study, four types of commercially available hydrophobic materials were selected as the coating materials. These hydrophobic materials are extremely convenient to use, and can be applied on a metal surface by a dip, spray or brush method. Stainless steel 304 is employed as the metal substrate owing to its common use in electromechanical drilling. The water contact angle of each coating sample was measured to characterize the surface water repellency. An ice adhesion measurement apparatus was designed to measure the ice adhesion strength, including the tensile (perpendicular to the interface) and shear (parallel to the interface) strengths. Considering the state of the electromechanical drill, the ice adhesion strengths on planar and curved surfaces with different coatings were tested at different temperatures. Subsequently, these tests were repeated, reusing each coating sample by growing new ice on it after detachment of the previous ice sample, allowing the deterioration in the performance of the coating during use to be evaluated. Moreover, a series of special abrasion tests were conducted to assess the mechanical strength of each coating plate.

2. Experimental section

2.1. Materials

The four mature commercial hydrophobic coating materials tested in this study are listed in Table 1. All materials can be easily used on a metal surface using a dip, spray, brush or other method, as discussed above. Stainless steel pipes with an outer diameter of 127 mm and a thickness of 5 mm and stainless steel plates with a thickness of 5 mm were used as a standard substrate. Their surfaces were polished before being brushed with the coating materials.

2.2. Hydrophobicity measurement

The hydrophobicity of a material is generally evaluated based on the water contact angle between a drop of water and a solid surface. In this study, the water contact angle of each coating was measured using a sessile drop method with a DSA-100 drop shape analyzer (Krüss Company, Germany) at room temperature (about 22°C). During the testing, the video signal of the water droplet on each coating was recorded using a video camera at high resolution. The water contact angle was obtained through image acquisition and data analysis by drop analysis DSA3 software.

2.3. Ice adhesion strength testing and procedure

The ice adhesion measurement apparatus developed in this study is shown in Figure 1, which mainly consists of a base frame designed with two guide ways, an electric draw stem and a force gauge. The coating samples are clamped onto the substrate plate

https://doi.org/10.1017/jog.2020.33 Published online by Cambridge University Press

Table 1. Hydrophobic coating materials used in this study

Coating	Product name	Description	Factory
A	CS-100	Mixture of silica, fluorocarbon resin and polytrifluoroethylene	Wuxi Youbo Chemical Co., Ltd., China
B	GF-2200	Modified Teflon	Dongguan Guangfu Chemical Co., Ltd., China
C	ZXL-DS-01	Silica-based emulsion	Laiyang Zixilai Environmental Protection Co., Ltd., China
D	DS-200	Copolymer of acrylic and perfluorinated ethylene	Dongguan Deshenglong Paint Co., Ltd., China

of the base frame. A cylindrical stainless steel sleeve with an inner diameter of 60 mm is set on the surface of the test coating sample, and a stainless steel cover connected with the force gauge is screwed on its top end. One large hole is designed on the cover so that distilled water can be easily deposited into the sleeve for freezing with a 40 mL syringe. During testing, the sleeve can be pushed and pulled by an electric draw stem at a constant speed of 7 mm s^{-1}. In addition, ice is removed from the interface between the ice and test surface of the coating samples. The maximum force applied to break the contact is measured and

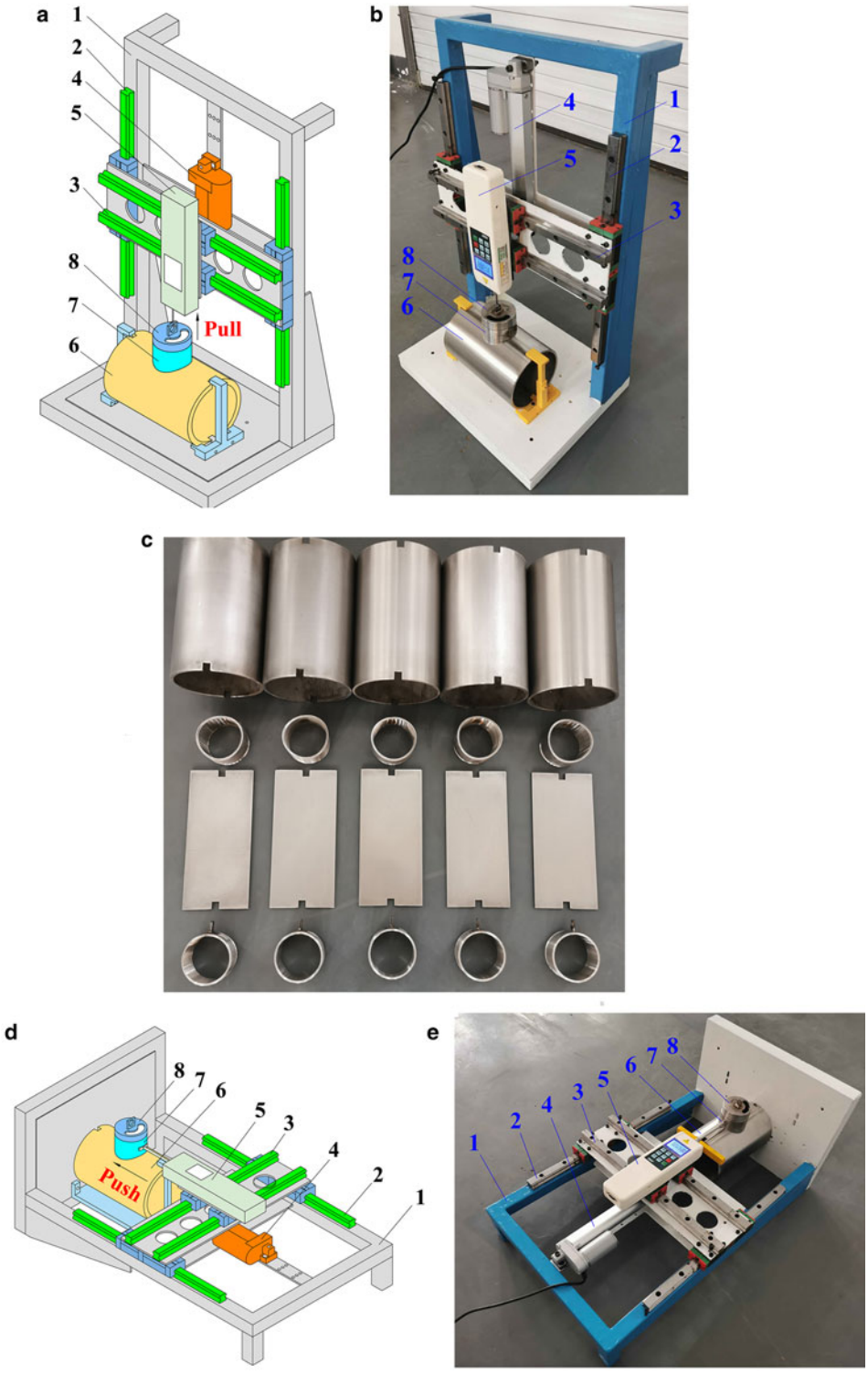

Fig. 1. Schematic illustration of ice adhesion measurement apparatus: (a) tensile force testing; (b) image of tensile force testing; (c) coating samples; (d) shear force testing; (e) image of shear force testing: (1) base frame; (2) guide way; (3) guide way; (4) electric draw stem; (5) force gauge; (6) coating samples; (7) stainless steel sleeve; and (8) stainless steel cover.

https://doi.org/10.1017/jog.2020.33 Published online by Cambridge University Press

recorded by a force gauge, and is then divided by the cross-sectional area of the ice–substrate interface to obtain the ice adhesion strength. The force gauge can move along the guideway to adjust its position to ensure that the force remains perpendicular or parallel to the test surface. When the ice adhesion force is larger than 200 N, an HF-1000 type force gauge with a range of 0–1000 N and a precision of 1 N is used. However, if the ice adhesion force is smaller than 200 N, an HF-200 force gauge is adopted to increase the measurement accuracy. The range and precision of the HF-200 force gauge are ~0–200 and 0.1 N, respectively. The entire experiment was conducted in a cold room, where the temperature can be adjustable at the range of 0 to −30°C with an increment of 0.1°C. Before testing, a cylinder sleeve with a cover and the coating samples are kept in a cold room for several hours to avoid the influence of the initial temperature on the test results. In addition, distilled water is stored at near 0°C for at least 1 h before being poured into the pre-chilled cylinder sleeves. Thus, a sealer between the sleeve and coating samples is not needed because the water is immediately solidified within the sleeve. The water is frozen for 4 h in the sleeve, which will be discussed later. After the water turns into ice, an external force is applied in the normal and shear directions to measure the ice adhesion strength. Five trials are conducted for each coating sample for a reliable measure of the mean and std dev. of the test results.

2.4. Durability measurement of the coatings

Undoubtedly, the durability and mechanical robustness of the coating play a significant role in the anti-icing property of an electromechanical drill because friction between the drill and ice is inevitable during its operation. Based on a study by Liu and others (2017), a method for evaluating the mechanical robustness of each coating is shown in Figure 2. The coating sample with a 100 g weight on top was placed on 2000 grit dry sandpaper and moved back and forth on the sandpaper by an electric draw stem. The speed and displacement of each movement were ~30 mm s^{-1} and 150 mm, respectively. After every ten abrasion cycles, the contact angle of each coating was measured to assess its durability. For simplicity and convenience, only the coatings on the planar surfaces were tested by the method described in this study.

Moreover, to evaluate the deterioration of the coating materials and estimate their practical application, the shear adhesion strength testing for each coating on a curved surface was repeated under the condition of continuous icing and de-icing cycles at −10°C.

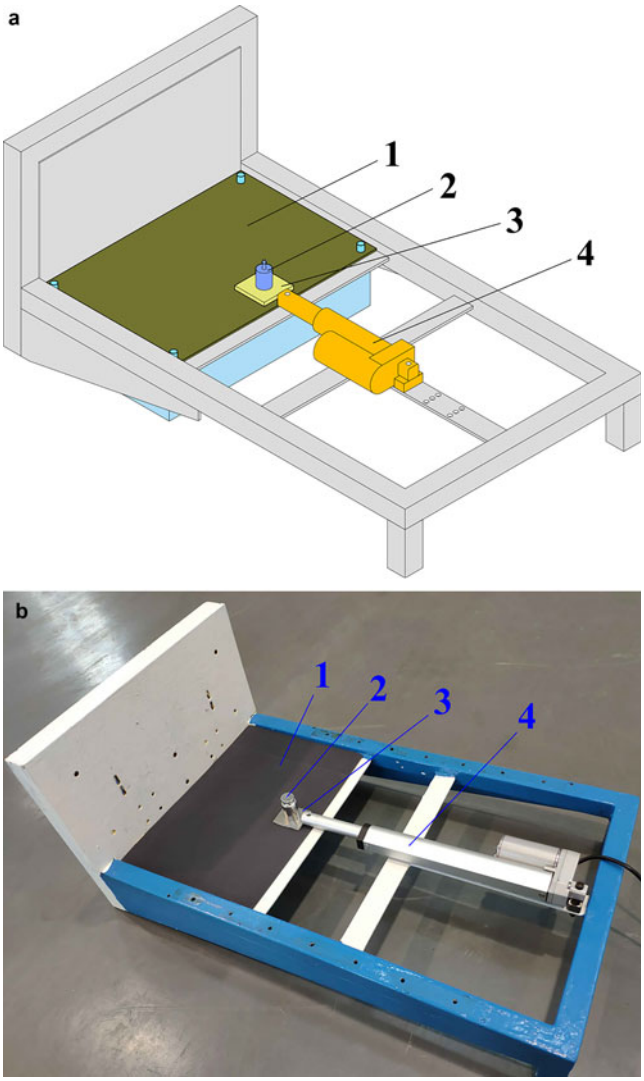

Fig. 2. Coating abrasion testing device: (a) abrasion testing; (b) image of the actual device: (1) sandpaper; (2) weight; (3) coating plate; (4) electric draw stem.

Table 2. Water contact angle value of the coating materials

Coating material	Bare metal plate	*A*	*B*	*C*	*D*
Water contact angle, °	76	107	101	114	95

3. Results and discussion

3.1. Water contact angle

The water contact angle value of each coating material on a stainless steel substrate is shown in Table 2. Coating *C* has the largest water contact angle, followed by coating *A*, with coating *D* being the smallest. Although these coatings are not as superhydrophobic as the manufacturers claimed, they did exhibit a substantial hydrophobicity because all their water contact angles are larger than 90°. The reason for the discrepancy may be the different substrate materials used.

3.2. Frozen time

It is evident that the ice accumulated on the coating samples and sleeves needs to be removed after each test. In this study, a natural melting method is adopted to remove this ice. That is, the coating samples and sleeves are placed in an outdoor environment after each test for several hours to let the ice gradually melt in a relatively warmer environment, and then placed in a cold room for cooling. The subsequent tests cannot be conducted until the surface temperature of these devices is returned to a value close to the ambient test temperature to avoid the initial surface temperature of the devices from influencing the ice adhesion strength. The curves of the change in surface temperature of the stainless steel plate during the cooling process are recorded using a Pt-100 type thermoresistor, the results of which are shown in Figure 3. It is seen that the surface temperature of the stainless steel plate first decreases rapidly owing to the large temperature difference, and the cooling rate then slows down when its temperature reaches the ambient temperature. After ~3.5 h of cooling, the surface temperature of the stainless steel plate can be considered the same as the ambient temperature. This means that the coating samples and sleeves should be cooled in the testing environment for no less than 3.5 h to avoid the influence of the initial temperature. In this

https://doi.org/10.1017/jog.2020.33 Published online by Cambridge University Press

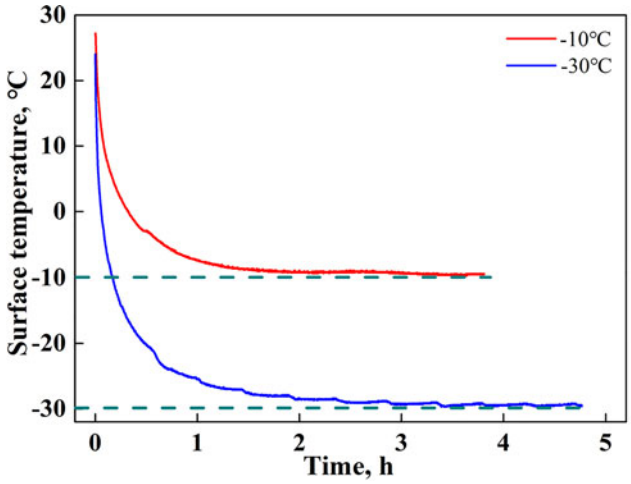

Fig. 3. Changes in the surface temperature of the stainless steel plate during the cooling process.

study, all devices were maintained at the test temperature for 6 h prior to freezing the ice.

Figure 4 illustrates the relationship between the tensile adhesion strength and the freezing time under a cooling condition of −10°C. It is apparent that the water should be frozen for at least 3 h to adhere to the substrate steadily for all coating samples in the environment at −10°C. If the ambient temperature is lower, the freezing process should be further accelerated. Based on this, the freezing time of water in this study is ∼4 h during all tests. In addition, the experiments show a better repeatability, although some documents have mentioned that freezer ice can lead to a relatively high error (Laforte and Beisswenger, 2005), which may be attributed to the use of a cold room and pure distilled water.

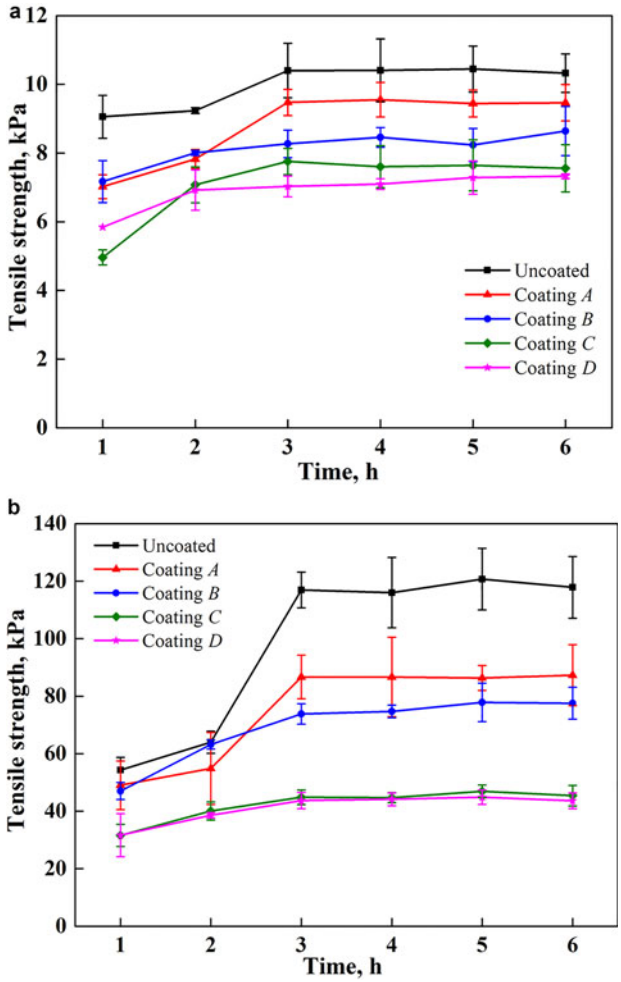

Fig. 4. Relationship between tensile adhesion force and freezing time (at −10°C): (a) planar surface (stainless steel plates); (b) curved surface (stainless steel pipes).

3.3. Ice adhesion strength

3.3.1. Ice adhesion on planar surface

The tensile and shear strengths of the ice adhesion on stainless steel plates with different coating samples at different testing temperatures are shown in Figure 5. It is clearly seen that the commercial hydrophobic coatings can more effectively reduce the ice adhesion compared to the bare stainless steel substrate. The lower the ambient temperature is, the more obvious these effects are. At an ambient temperature of −10°C, the average tensile strength of ice adhesion on an uncoated surface is ∼9.65 kPa, whereas it is reduced to 9.43, 7.97, 7.72 and 7.17 kPa on surface coatings *A*, *B*, *C* and *D*, respectively. When the ambient temperature decreases to −30°C, it increases to ∼14.01 kPa on an uncoated surface, whereas it is ∼11.47, 9.76, 7.72 and 1.81 kPa on surface coatings *A*, *B*, *C* and *D*, respectively, as shown in Figure 5a. Therefore, coating *D* exhibits excellent anti-icing properties among the four coatings applied. Compared with the uncoated surface, it can reduce the tensile strength by 25.70% at −10°C and 87.08% at −30°C, respectively. This is followed by coating *C*, which decreases the tensile strength by 20.00% at −10°C and by 44.90% at −30°C. The anti-icing performance of coating *A* is the worst.

The variation trend of the shear adhesion strength on the different coatings is similar to that of the tension strength, but its value is larger, as shown in Figure 5b. Among the four types of coatings, the shear strength of ice adhered on coating *D* is the smallest. Compared with the uncoated surface, this coating can reduce the shear strength of ice adhesion by ∼60.25% at −10°C and 97.11% at −30°C. The next is coating *C*, which can decrease the shear strength to ∼5.37 and 13.24 kPa at −10 and −30°C, respectively.

It is worth noting that there seems to be no connection between the water contact angle and the ice adhesion strength. The water contact angle of coating *C* is the largest, whereas its ice adhesion strength is not the lowest. Coating *D* has the least ice adhesion strength, but its water contact angle is also the lowest.

Moreover, it is clear from Figure 5 that the ambient temperature is an important influential parameter for the ice adhesion strength on a planar surface. With decrease in the ambient temperature, the ice adhesion strength increases with an approximately linear dependence for an uncoated surface and the coating samples *A* and *B*. These trends are similar to that of previous studies on hydrophobic surfaces (Soltis and others, 2015; Janjua, 2017). The reason for this may be the fracturing of ice from these substrate surfaces through a combination of adhesive and cohesive breaks, based on the residual ice observed on the surfaces of the uncoated surface and coating *A* at all five testing temperatures and that observed from −20°C on coating *B* samples, as shown in Figure 6. In most cases, a lower temperature produces a higher strength of ice. Therefore, the ice adhesion strength increases with a decrease in temperature. For the coating samples *C* and *D*, the fracture of ice is a pure adhesive break at all testing temperatures because the surfaces are relatively smooth after the ice is detached. In addition, the ice adhesion strength on coating *D*

https://doi.org/10.1017/jog.2020.33 Published online by Cambridge University Press

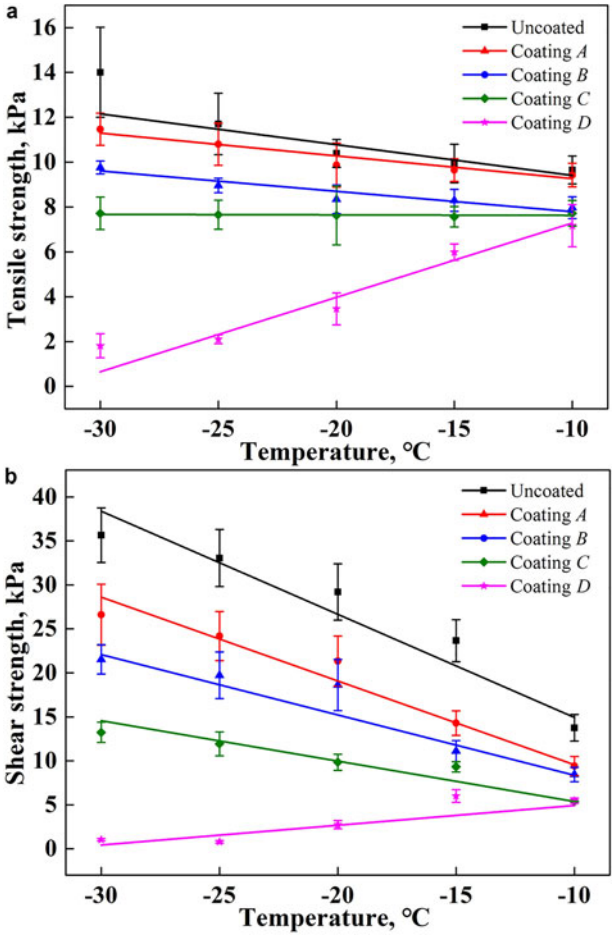

Fig. 5. Ice adhesion strength on planar surfaces with different coating materials over a range of temperatures: (a) tensile strength of ice adhesion; (b) shear strength of ice adhesion.

is decreased with a decline in temperature. This may have occurred because the lower temperature increases the ice-freezing rate, which results in a lower adhesion force, although this requires further study.

3.3.2. Ice adhesion on curved surface

Figure 7 shows the results of the ice adhesion strength on curved surfaces with different coating samples. It is seen that the variation in the ice adhesion strength on curved surfaces with a change in temperature is similar to that on planar surfaces, although the values are much higher. When the ambient temperature decreases from −10 to −30°C, the average tensile strength of ice adhesion increases from 115.20, 86.23, 51.93 and 45.33 kPa to 226.72, 178.49, 111.24 and 78.97 kPa on an uncoated surface, and on sample coatings *A*, *B* and *C*, respectively. However, it is reduced from 44.21 to 4.39 kPa on the coating *D* substrate, which decreased by 61.62 and 98.06% compared with the uncoated surface.

The shear strength of ice adhesion on coating *D* substrate is also the smallest among all tested samples, varying from 7.01 to 55.76 kPa. On the uncoated surface, however, it is much higher, ranging from 122.73 to 182.16 kPa. Therefore, coating *D* demonstrates an excellent anti-icing property even on a curved surface, which can reduce the ice shear adhesion strength by nearly 54.57 and 96.15% at −10 and −30°C, respectively, compared to an uncoated surface.

Furthermore, although a pure adhesive fracture occurred on the surfaces of sample coatings *C* and *D* at all tested temperatures, such fracturing occurred only under a combination of cohesive and adhesive forces for the uncoated surface and coating *A*, as shown in Figure 8. For coating *B*, the change in ice fracture behavior is observed at −15°C.

3.4. Coating durability

To better understand the mechanical durability of each coating tested in this study, we conducted abrasion tests as discussed above. The change in water contact angle was measured after every ten cycles, the results of which are shown in Figure 9. Coating *A* has the worst abrasion resistance because its water contact angle decreases to ~90° after only 100 cycles of abrasion. For the three other coatings, the abrasion resistance showed little change, and the water repellency is lost after ~140 cycles of abrasion. In addition, the performance of coating *D* is relatively stable despite its water contact angle being the smallest among all coatings. After 80 cycles of abrasion, its water contact angle remained at 95°, which is almost the same as its initial value.

Figure 10 shows the change in the shear strength of ice adhered on the curved surfaces at −10°C with different icing and de-icing cycles. Although hydrophobic coatings can significantly reduce the ice adhesion strength and prevent ice accumulation, their durability is the most difficult challenge in a practical application, as shown in Figure 10. After repeated icing and de-icing, all coated samples show a gradual increase in ice adherence. For coating *A*, the shear force increases to ~110.33 kPa after

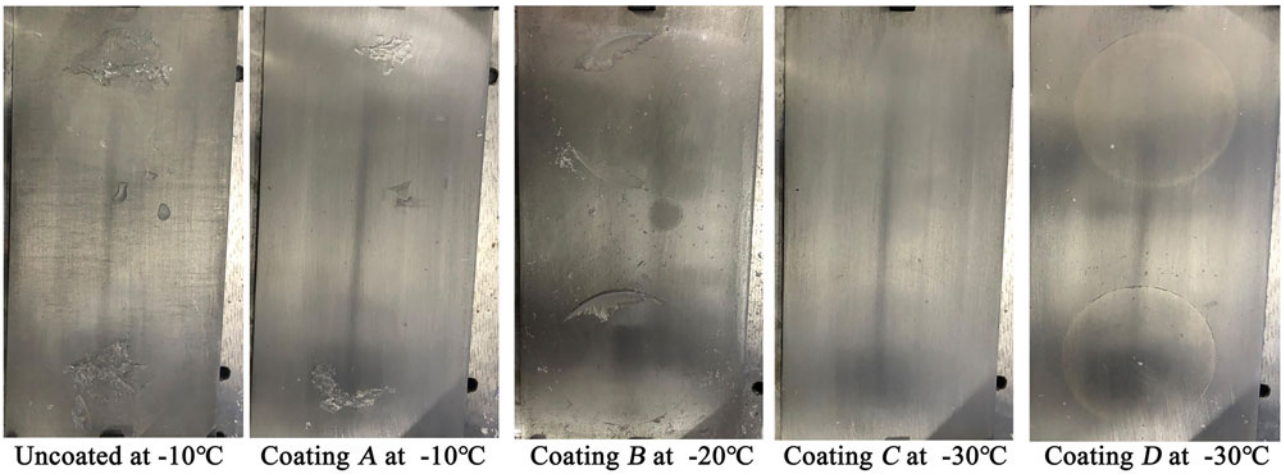

Fig. 6. Fracture surface of the ice on planar surfaces with different coating samples.

https://doi.org/10.1017/jog.2020.33 Published online by Cambridge University Press

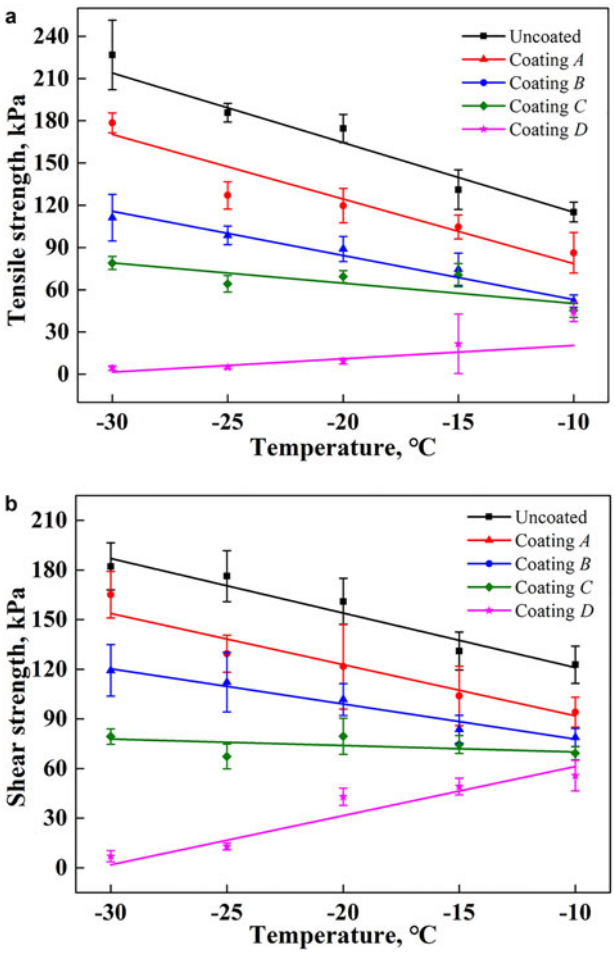

Fig. 7. Ice adhesion strength on curved surfaces with different coating materials over a range of temperatures: (a) tensile strength of ice adhesion; (b) shear strength of ice adhesion.

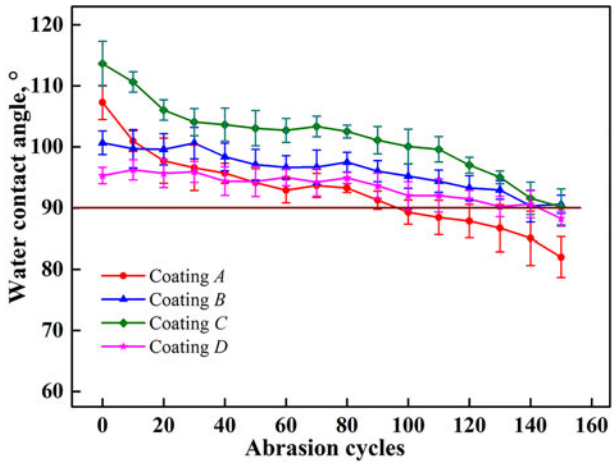

Fig. 9. Water contact angles of hydrophobic coating surfaces versus abrasion cycles.

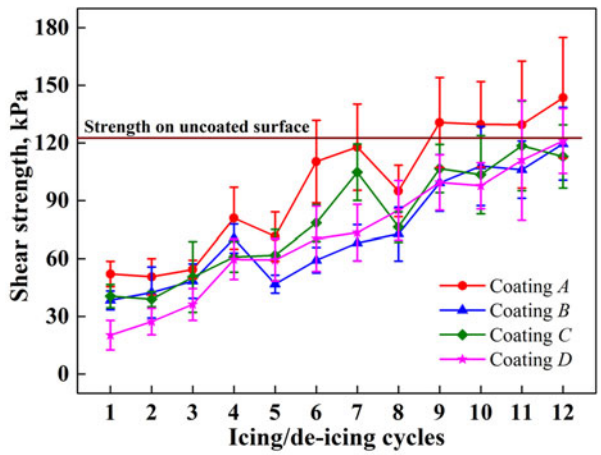

Fig. 10. Shear strength of ice detachment from the curved surface at −10°C versus icing/de-icing cycles.

six cycles of icing and de-icing experiments, which is slightly lower than that on the uncoated surface at ~122.73 kPa. For the other three coatings, the shear strengths are close to that on the uncoated surface after 11 cycles. According to previous reports on various hydrophobic and superhydrophobic surfaces, these increases in ice adhesion strength are attributed to a larger ice-solid contact area on the surfaces after several icing and de-icing tests (Farhadi and others, 2011).

Based on the results shown in Figures 9 and 10, coatings *C* and *D* maybe not be sufficiently strong for use on the cutting surface of the electromechanical drill because a large amount of friction is generated between the ice and cutters during ice drilling. This needs to be further tested and analyzed. For other parts of the drill, the service life of these two coatings should not be a problem because little friction occurs there. Together, coatings *C* and *D*

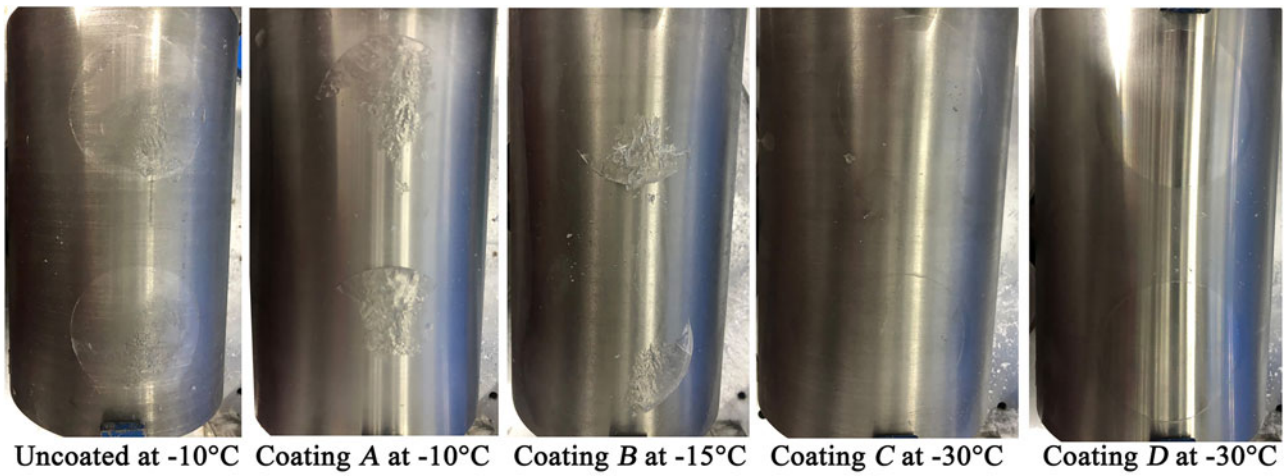

Fig. 8. Fracture surface of the ice on curved surfaces with different coating samples.

https://doi.org/10.1017/jog.2020.33 Published online by Cambridge University Press

achieve a good anti-icing performance, and can greatly reduce the ice adhesion strength, allowing an effective decrease in or complete prevention of stuck drills in warm ice when using an electromechanical drill. Therefore, applying a coating of hydrophobic material on a drill surface is believed to be a promising method for solving the difficulties of warm ice drilling, although its anti-icing capabilities need to be further studied.

4. Conclusions and perspectives

An ice adhesion testing instrument was developed to assess the ice adhesion characteristics of different hydrophobic coatings on metallic substrates. Four different types of commercially available hydrophobic coating materials were chosen to coat the surfaces of a stainless steel surface: a mixture of silica and fluorocarbon resin with polytrifluoroethylene, modified Teflon, silica-based emulsion and an acrylic-based copolymer. The tensile and shear strengths of ice detached from planar and curved surfaces coated with these hydrophobic materials were measured. The conclusions derived from this study are as follows.

(1) All four coatings demonstrate a certain water repellency property with water contact angles of 107°, 101°, 114° and 95°, respectively.
(2) Compared with bare stainless steel surfaces, all four coatings can effectively reduce the ice adhesion strength on either a planar or curved surface. The lower the ambient temperature is, the greater the effect. In addition, the coating of an acrylic-based copolymer has the best anti-icing property among the four tested coatings. Compared with an uncoated surface, it can reduce the mean tensile strength and shear stress by 87.08 and 97.11% on a planar surface at −30°C, and by 98.06 and 96.15% on a curved surface, respectively. The effect of a silica-based emulsion is slightly worse than that of an acrylic-based copolymer coating in terms of the anti-icing performance, followed by modified Teflon. In addition, for the coating of an acrylic-based copolymer and silica-based emulsion, the fracture behavior of ice adhered to its surface is purely adhesive, whereas for other types of coatings, it is a combination of an adhesive and cohesive break.
(3) Although all hydrophobic coatings tested in this study can significantly reduce the ice adhesion strength over an uncoated surface, their water repellency and anti-icing performances gradually decrease with use. The water repellency is lost after ∼140 cycles of abrasion for both an acrylic-based copolymer and a silica-based emulsion. Moreover, the shear strengths of ice adhered to a curved surface will be close to that on an uncoated surface after 11 cycles of icing and de-icing for both coatings at −10°C.

The use of hydrophobic or superhydrophobic materials to coat the surfaces of an electromechanical drill and prevent ice from accreting on its surfaces, particularly on the cutters, coring head and core barrel, may be a promising method to solve the difficulties incurred during warm ice drilling. Next, an acrylic-based copolymer and a silica-based emulsion will be coated on the surface of an electromechanical drill in a future study. An ice borehole will be drilled in a laboratory to study the actual effectiveness of the anti-icing and real service life of these two hydrophobic materials.

Acknowledgements. The authors thank the anonymous reviewers and the editor for their useful remarks and comments. This study was supported by the National Natural Science Foundation of China (project no. 41576184). The authors declare that there is no conflict of interest.

References

Augustin L and 6 others (2007) Drilling comparison in 'warm ice' and drill design comparison. *Annals of Glaciology* **47**, 73–78. doi: 10.3189/172756407786857820.

Barthlott W and Neinhuis C (1997) Purity of the sacred lotus, or escape from contamination in biological surfaces. *Planta* **202**(1), 1–8. doi: 10.1007/s004250050096.

Bernagozzi I, Antonini C, Villa F and Marengo M (2014) Fabricating superhydrophobic aluminum: an optimized one-step wet synthesis using fluoroalkyl silane. *Colloids and Surface A: Physicochemical and Engineering Aspects* **441**, 919–924. doi: 10.1016/j.colsurfa.2013.05.042.

Bharathidasan T, Vijay Kumar S, Bobji MS, Chakradhar RPS and Basu BJ (2014) Effect of wettability and surface roughness on ice-adhesion strength of hydrophilic, hydrophobic and superhydrophobic surfaces. *Applied Surface Science* **314**, 241–250. doi: 10.1016/j.apsusc.2014.06.101.

Cao PL, Chen BY, Liu CP, Yang C and Talalay P (2015) Experimental investigation of cutting temperature in ice drilling. *Cold Regions Science and Technology* **116**, 78–85. doi: 10.1016/j.coldregions.2015.04.008.

Cao LL, Jones AK, Sikka VK, Wu JZ and Gao D (2009) Anti-icing superhydrophobic coatings. *Langmuir* **25**(21), 12444–12448. doi: 10.1021/la902882b.

Cao PL, Liu MM, Chen Z, Chen BY and Zhao Q (2018) Theory calculation and testing of air injection parameters in ice core drilling with air reverse circulation. *Polar Science* **17**, 23–32. doi: 10.1016/j.polar.2018.06.005.

Chen WM and 7 others (2018) Fast formation of hydrophobic coating on wood surface via an energy-saving dielectric barrier discharges plasma. *Progress in Organic Coatings* **125**, 128–136. doi: 10.1016/j.porgcoat.2018.06.018.

Farhadi S, Farzaneh M and Kulinich SA (2011) Anti-icing performance of superhydrophobic surfaces. *Applied Surface Science* **257**(14), 6264–6269. doi: 10.1016/j.apsusc.2011.02.057.

Fillion PM, Riahi AR and Edrisy A (2014) A review of icing prevention in photovoltaic devices by surface engineering. *Renewable Sustainable Energy Reviews* **32**, 797–809. doi: 10.1016/j.rser.2014.01.015.

Guerin F, Laforte C, Farinas M and Perron J (2016) Analytical model based on experimental data of centrifuge ice adhesion tests with different substrates. *Cold Regions Science and Technology* **121**, 93–99. doi: 10.1016/j.coldregions.2015.10.011.

Hasegawa T, Aizawa T, Inohara T, Wasa K and Anzai M (2018) Hot mold stamping of optical plastics and glasses with transcription of superhydrophobic surfaces. *Procedia Manufacturing* **15**, 1437–1444. doi: 10.1016/j.promfg.2018.07.337.

He Y and 5 others (2015) Reducing ice accumulation and adhesion by using a flexible micro-rod film. *Cold Regions Science and Technology* **118**, 57–63. doi: 10.1016/j.coldregions.2015.06.001.

Hu ZS and Deng YL (2010) Superhydrophobic surface fabricated from fatty acid-modified precipitated calcium carbonate. *Industrial & Engineering Chemistry Research* **49**(12), 5625–5630. doi: 10.1021/ie901944n.

Janjua ZA (2017) The influence of freezing and ambient temperature on the adhesion strength of ice. *Cold Regions Science and Technology* **140**, 14–19. doi: 10.1016/j.coldregions.2017.05.001.

Johnsen SJ and 16 others (2007) The Hans Tausen drill: design, performance, further developments and some lessons learned. *Annals of Glaciology* **47**, 89–98. doi: 10.3189/172756407786857686.

Jung M and 7 others (2015) Design and fabrication of a large-area superhydrophobic metal surface with anti-icing properties engineered using a top-down approach. *Applied Surface Science* **352**, 920–926. doi: 10.1016/j.apsusc.2015.06.024.

Kim K, Lichtenhan JD and Otaigbe JU (2019) Facile route to nature inspired hydrophobic surface modification of phosphate glass using polyhedral oligomeric silsesquioxane with improved properties. *Applied Surface Science* **470**, 733–743. doi: 10.1016/j.apsusc.2018.11.181.

Laforte C and Beisswenger A (2005) Icephobic material centrifuge adhesion test. In *11th International Workshop on Atmospheric Icing on Structures*, Montreal, Canada.

Liu XL, Chen HW, Kou WP and Zhang DY (2017) Robust anti-icing coatings via enhanced superhydrophobicity on fiberglass cloth. *Cold Regions Science and Technology* **138**, 18–23. doi: 10.1016/j.coldregions.2017.03.004.

Liu ZL, Gou YJ, Wang JT and Cheng SY (2008) Frost formation on a superhydrophobic surface under natural convection conditions. *International Journal of Heat and Mass Transfer* **51**(25–26), 5975–5982. doi: 10.1016/j.ijheatmasstransfer.2008.03.026.

Matoba S, Shimbori K and Shiraiwa T (2014) Alpine ice-core drilling in the North Pacific region. *Annals of Glaciology* **55**(68), 83–87. doi: 10.3189/2014aog68a020.

Motoyama H (2007) The second deep ice coring project at Dome Fuji, Antarctica. *Scientific Drilling* **5**, 41–43. doi: 10.5194/sd-5-41-2007.

Murshed MM, Faria SH and Kuhs WF (2007) The role of hydrochlorofluorocarbon densifiers in the formation of clathrate hydrates in deep boreholes and subglacial environments. *Annals of Glaciology* **47**, 109–114. doi: 10.3189/172756407786857659.

Park Y and 6 others (2019) Heat transfer augmentation in two-phase flow heat exchanger using porous microstructures and a hydrophobic coating. *Applied Thermal Engineering* **153**, 433–447. doi: 10.1016/j.applthermaleng.2019.03.030.

Popp TJ, Hansen SB, Sheldon SG and Panton C (2014b) Deep ice-core drilling performance and experience at NEEM, Greenland. *Annals of Glaciology* **55**(68), 53–64. doi: 10.3189/2014AoG68A042.

Popp TJ, Hansen SB, Sheldon SG, Schwander J and Johnson JA (2014a) Drilling into debris-rich basal ice at the bottom of the NEEM (Greenland) borehole. *Annals of Glaciology* **55**(68), 199–206. doi: 10.3189/2014AoG68A029.

Soltis J, Palacios J, Eden T and Wolfe D (2015) Evaluation of ice-adhesion strength on erosion-resistant materials. *AIAA Journal* **53**(7), 1825–1835. doi: 10.2514/1.j053516.

Talalay P and 7 others (2015) Ice-core drilling problems and solutions. *Cold Regions Science and Technology* **120**, 1–20. doi: 10.1016/j.coldregions.2015.08.014.

Vasiliev NI and 8 others (2007) Deep drilling at Vostok station, Antarctica: history and recent events. *Annals of Glaciology* **47**, 10–23. doi: 10.3189/172756407786857776.

Zagorodnov V, Thompson LG, Ginot P and Mikhalenko V (2005) Intermediate-depth ice coring of high-altitude and polar glaciers with a lightweight drilling system. *Journal of Glaciology* **51**(174), 491–501. doi: 10.3189/172756505781829269.

https://doi.org/10.1017/jog.2020.33 Published online by Cambridge University Press